



Influence of operating conditions on the optimum design of electric vehicle battery cooling plates



Anthony Jarrett, Il Yong Kim*

Queen's University, Kingston, Ontario, Canada K7L 3N6

HIGHLIGHTS

- A battery cooling plate was modelled parametrically and assessed using CFD.
- Numerical optimization was applied to improve its design.
- Design sensitivity of the optimum design to the boundary conditions was assessed.
- Temperature uniformity optimizations were most sensitive.
- Battery heat flux magnitude and coolant flow rate had negligible effect.

ARTICLE INFO

Article history:

Received 11 April 2013

Received in revised form

19 June 2013

Accepted 20 June 2013

Available online 10 July 2013

Keywords:

Electric vehicle battery

Cooling plate

Coolant flow channel

Thermal management

Temperature uniformity

Design optimization

ABSTRACT

The efficiency of cooling plates for electric vehicle batteries can be improved by optimizing the geometry of internal fluid channels. In practical operation, a cooling plate is exposed to a range of operating conditions dictated by the battery, environment, and driving behaviour. To formulate an efficient cooling plate design process, the optimum design sensitivity with respect to each boundary condition is desired. This determines which operating conditions must be represented in the design process, and therefore the complexity of designing for multiple operating conditions. The objective of this study is to determine the influence of different operating conditions on the optimum cooling plate design. Three important performance measures were considered: temperature uniformity, mean temperature, and pressure drop. It was found that of these three, temperature uniformity was most sensitive to the operating conditions, especially with respect to the distribution of the input heat flux, and also to the coolant flow rate. An additional focus of the study was the distribution of heat generated by the battery cell: while it is easier to assume that heat is generated uniformly, by using an accurate distribution for design optimization, this study found that cooling plate performance could be significantly improved.

© 2013 Elsevier B.V. All rights reserved.

1. Introduction

Adequate temperature control of electric vehicle (EV) batteries is vital for their efficient operation, maximum lifetime, and safety. Operation at elevated temperature causes battery degradation through increased rate of corrosive reactions; operation at low temperature suppresses the electro-chemical reactions leading to reduced power output [1]. As an EV is a closed system, all power required for the operation of a thermal management system will directly reduce the power available to the primary vehicle

functions; therefore it is also a requirement that the power consumption be as low as possible [2].

A common battery pack configuration is a stack of rectangular laminate battery cells; in this design, temperature control can be provided by including cooling plates between battery cells. These are thin metal fabrications with internal channels through which a coolant flows. Heat generated in the battery cells is conducted into the cooling plate and then into the cooling plate at a rate determined by the heat generation rate in the cell. The heat is transported by the coolant away from the battery and discarded outside of the battery.

Previous studies have measured the heat generated by lead-acid cells [1–3], nickel–zinc cells [3], and lithium ion cells [3,4] used for powering electric vehicles. In all studies, there was significant variation depending on battery temperature, discharge

* Corresponding author.

E-mail addresses: tony_jarrett@hotmail.com (A. Jarrett), iykim@me.queensu.ca (I.Y. Kim).

rate, and state of charge (SOC). Low temperatures and fast discharge rates tend to result in a higher heat generation rate [3]. Typical values for Li-ion cells during representative driving profiles were measured at an average of between 2 and 20 W per cell, with peaks up to 50 W [4].

The spatial heat generation distribution in an EV battery cell has been assessed both empirically and analytically. Pesaran et al. [1,3] have utilized thermal imaging to measure the temperature of various battery cells under different conditions. The temperature distribution was highly dependent on the battery chemistry and geometry: cylindrical lead-acid cells showed a strong temperature concentration near the terminals, but cuboid nickel–zinc cells had the highest temperature in the body away from the terminals. Kim et al. [5] used numerical modelling to simulate the electro-chemical reactions in a rectangular laminate Li-ion cell, validated with thermal imaging. They found a significant temperature concentration around the terminals, resulting in a marked temperature gradient across the cell. Furthermore, due to prolonged temperature non-uniformity, the cell could suffer from non-uniform degradation, which will alter the distribution of heat generation [6]. The cooling plate could therefore experience non-uniform conduction from the battery cell, in a pattern that shifts over the life of the battery.

In addition to the influence of operation on the thermal behaviour, the reverse also needs consideration: the thermal condition of the battery affects its operating parameters. Battery SOC decreases more rapidly in cold conditions, and so less energy is available to the vehicle [7]. Elevated battery temperature is a contributing factor to long-term loss in capacity through material degradation and increase in impedance [6].

Controlling the battery operation to achieve the desired combination of thermal behaviour, performance, and durability is the role of the battery management system (BMS). This requires mathematical models of the battery behaviour; for example, as derived by Hu et al. [8] for SOC estimation, or Kim et al. [9] for heat generation. In order to perform optimally given any battery condition and operating state, these models need to be comprehensive and robust.

In response to the vehicle operation, and dictated by the battery models, the BMS will control the flow of coolant to the battery pack to maintain an acceptable operating temperature, while minimizing the cooling system power consumption. In addition to the operating conditions and battery state, the flow rate required will depend on the battery pack configuration and the heat-exchange efficiency of the cooling system. Some indication of a typical flow rate is given by Jayaraman et al. [10] who discuss the simulation of the battery pack of the Chevrolet Volt: a representative analysis supplies each cooling plate with approximately $1 \times 10^{-6} \text{ m}^3 \text{ s}^{-1}$.

A previous study of the design of EV battery cooling plates by the authors [11] determined that the performance of the cooling plate can be optimized by modifying the geometry of the coolant channel, and that different designs are required depending on the objective function. However, this study used a single set of fixed boundary conditions, whereas it has been demonstrated that a cooling system must function robustly at a range of different boundary conditions. Furthermore, this previous study assumed a uniform distribution of heat generated by the battery.

Other studies on the specific subject of EV battery cooling plates are sparse, and so conclusions must be extrapolated from the similar fields of electronics cooling and fuel cell cooling. Yu et al. [12] used computational fluid dynamics (CFD) to assess several fuel cell cooling plate designs with respect to temperature uniformity over a range of flow rates and heat generation magnitudes. Variation in the magnitude of heat generation influenced temperature uniformity, but the relative performance of different cooling plate

designs remained unchanged. Conversely, changes in the coolant flow rate did affect the relative efficacy of the cooling plate designs. This indicates that the optimum design at one heat generation rate will also be the optimum design at other rates of heat generation, but if the coolant flow rate is changed, a different design would be required in order to perform optimally.

The cooling of high power electronics can be achieved using a heatsink with internal channels carrying a coolant. These are typically straight, parallel channels, and so their performance can be approximated using analytical methods. Bau [13] determined that the optimum channel geometry for reducing the maximum temperature, and for minimizing the temperature gradient are different. Furthermore, the flow rate and thermal properties of the coolant also affect the optimum geometry. However, the different scale and boundary conditions make the conclusions of this study difficult to apply directly to the design of EV battery cooling plates.

It has been established that the geometry of EV cooling plates can be optimized with respect to specific objective functions, and that in similar liquid cooled systems, the boundary conditions can affect the optimum design. However, there has been no study on optimum and robust cooling plate design with respect to variability in the boundary conditions such as the coolant flow rate. Furthermore, all previous studies have assumed a uniform distribution of heat generated, when in fact most battery cells have a significantly non-uniform distribution of heat.

The objective of this study is to determine the effect of varying the boundary conditions on the optimum cooling plate design. The variation of three types of boundary condition was considered: the coolant flow rate, and the magnitude and non-uniform distribution of heat generation.

We will look at this problem from two aspects. (1) The first is to study how the optimum design changes according to the variation of a boundary condition. After finding optimum solutions for all multiple different values of a boundary condition, we will discuss if there is a noticeable trend in the optimum design change according to the boundary condition variation. (2) The second is to determine the performance of an optimum design at off-design boundary conditions, that is when the optimum design is exposed to a boundary condition that is different from the one used to determine that optimum design. We can then have a discussion on the optimum design's robustness against boundary condition variation.

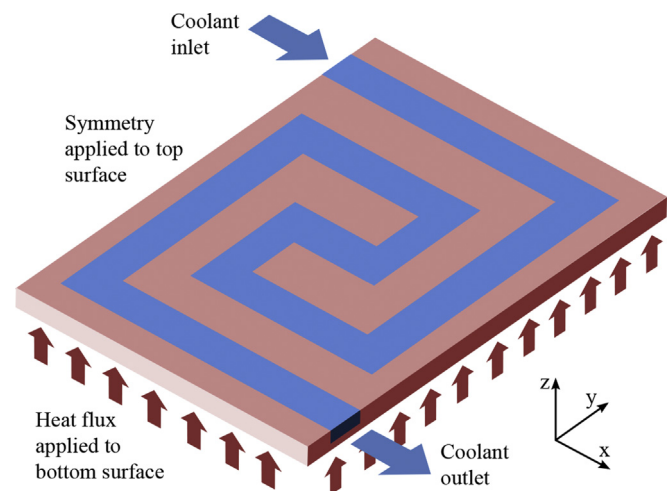


Fig. 1. Cooling plate CFD analysis. Coolant enters the plate at the top left corner with a constant mass flow rate; there is a zero-pressure outlet at the opposite corner. A heat flux boundary condition on the bottom face simulates the heat generated in the battery cell, and a symmetry condition is applied to the top face.

Table 1

Material properties of 50–50 ethylene glycol–water mix.

Property	Model	Value
Density (kg m^{-3})	Constant	1065
Specific heat ($\text{J kg}^{-1} \text{K}^{-1}$)	Polynomial	$2574.7 + 3.0655T$
Thermal conductivity ($\text{W m}^{-1} \text{K}^{-1}$)	Constant	0.42
Viscosity ($\text{kg m}^{-1} \text{s}^{-1}$)	Power law	$0.0069 \times (T/273)^{-8.3}$

2. Method

2.1. Cooling plate modelling and simulation

The cooling plate assessed in this study is a thin rectangular aluminium block with a single serpentine channel with a geometry based on the design of previous studies [11,12]. Coolant enters the channel at one side of the plate, and flows through the channel before leaving the plate from the other side. In operation it will be sandwiched between two battery cells, each generating heat which is conducted into the plate and then to the coolant. As it is symmetric in the thickness-wise direction, a half plate can be analyzed with a symmetry boundary condition. A parameterized model generation routine was used with the CFD pre-processor GAMBIT: this allows the creation of a cooling plate model in which the width and location of each section of the cooling channel can be specified independently. It was meshed with 243,560 hexahedral elements; testing showed that this size of mesh was sufficient to provide a reliable result [11].

The cooling plate was analyzed using the commercial CFD solver, FLUENT. The boundary conditions of the mass flow rate and coolant temperature were specified at the inlet, and a zero static pressure was specified at the outlet. A uniform heat flux was applied on the bottom surface as shown in Fig. 1. Material properties of a water–glycol mix were applied to the fluid, and aluminium to the solid regions of the plate. The material properties are listed in Table 1. The analysis was performed using verified laminar solution settings [11], after which output parameters were recorded. The three principal outputs were (1) the standard deviation of the temperature on the heat flux surface, (2) the average temperature on the same surface, and (3) the total pressures on the inlet and outlet surfaces (which are used to calculate the pressure drop).

2.2. Cooling plate optimization

The optimization algorithm was written in the MATLAB programming environment. This algorithm uses the sequential quadratic programming function, *fmincon*, to determine the optimum geometry of the cooling channel for any given objective function. The design variables for the optimization were the in-plane width and location of all nine sections of the cooling channel, with constraints to maintain a minimum section thickness: this allowed the cooling plate design to vary as indicated in Fig. 2. All

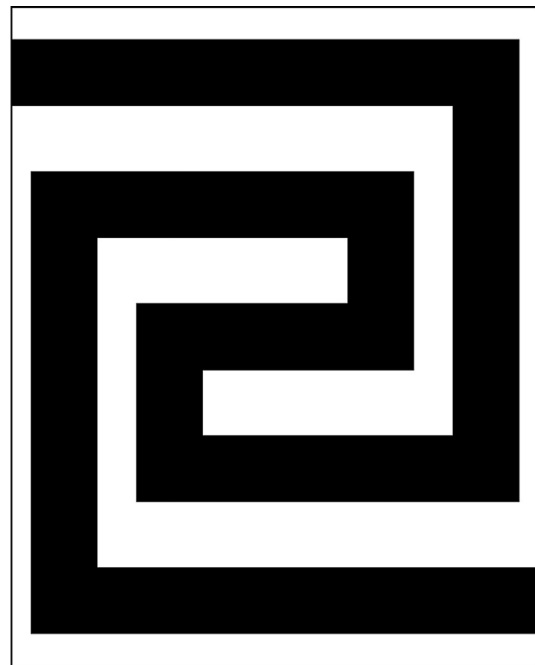


Fig. 3. Reference cooling plate geometry: used as initial design for optimization, and as reference for performance comparisons.

optimizations started from the same design: the reference cooling plate geometry is shown in Fig. 3.

The optimization used three separate objective functions: average plate temperature, T_{avg} ; standard deviation of temperature, T_{σ} ; and coolant pressure drop, P_{fluid} . The temperature objectives were measured on the face of the cooling plate with the heat flux boundary condition (the bottom surface in Fig. 1). The optimization algorithm was run for up to 100 design iterations, or until the objective function showed a change of no more than 0.001% in subsequent design iterations. Our previous work [11] has applied this algorithm to the optimization of this cooling plate with the boundary condition of 500 W m^{-2} uniform heat flux and 0.001 kg s^{-1} coolant flow rate. For effective comparison, these boundary conditions will be noted as ‘Reference BC’ in this study. Optimum designs for the three objective functions subject to Reference BC are shown in Fig. 4.

2.3. Boundary conditions

2.3.1. Heat flux distribution

As discussed in the Introduction, the spatial distribution of temperature in a battery cell varies significantly depending on the cell format and chemistry. It is not the purpose of this study to replicate any one pattern of heat generation, but rather we investigate its effect on the performance of a cooling plate. The thermal assessment of a rectangular laminate lithium-ion cell in the study

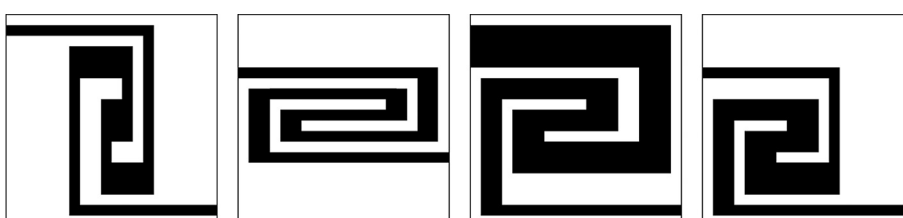


Fig. 2. Possible cooling plate geometry with variation in design variables (the coolant channel is shown in black).

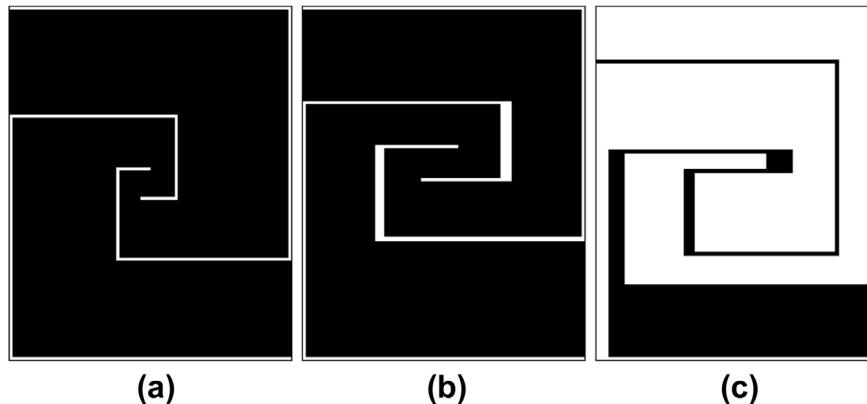


Fig. 4. Optimum cooling plate designs for 3 objective functions – pressure drop, average temperature, and temperature deviation – subject to Reference BC (500 W m⁻² uniform heat flux and 0.001 kg s⁻¹ coolant flow rate). The coolant channel is shown in black. (a) P_{fluid} optimized geometry. (b) T_{avg} optimized geometry (c) T_{σ} optimized geometry.

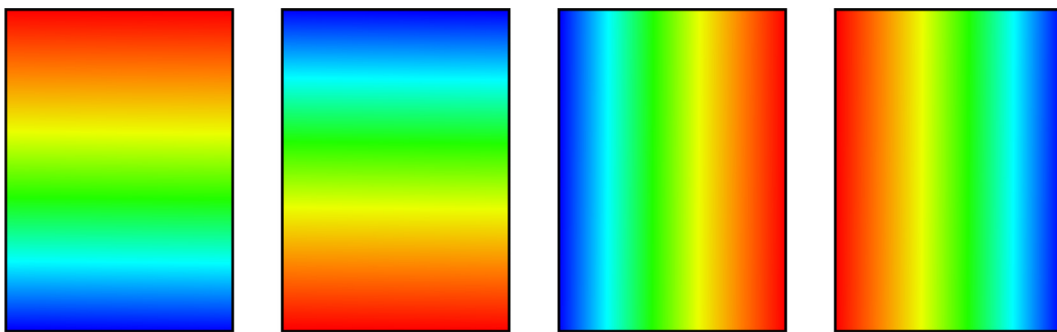


Fig. 5. Four linear heat flux gradients from 0 (blue) to 1000 W m⁻² (red). From left to right: +y, -y, +x, -x. +y indicates a heat flux whose magnitude increases linearly from zero in the direction of the positive y axis. (For interpretation of the references to colour in this figure legend, the reader is referred to the web version of this article.)

by Kim et al. [5] is particularly convenient, as it is the type that would find use in a battery pack with cooling plates. Their study showed that the highest temperature in the cell is at the top edge, where the connectors are located, and gradually decreases towards the bottom edge. The conversion from temperature distribution to heat generation distribution is non-trivial without additional information (transient details, surface convection, thermal properties), hence for simplicity this study assumed a linear gradient of heat flux increasing from zero. We considered four different directions of a linear gradient (positive and negative gradients in both the x and y directions); four cases with an average magnitude of 500 W m⁻² are shown graphically in Fig. 5.

The total heat generated by the battery was set at 16 W, based on values in literature and technical data from our industrial partner, General Motors (GM) of Canada. Based on the battery size, this is equivalent to a uniform heat flux of 500 W m⁻², or a linear gradient from 0 to 1000 W m⁻² (i.e. an average of 500 W m⁻²).

Optimization of the cooling plate was performed with respect to objective functions of T_{avg} and T_{σ} , for all four linear heat flux distributions, and also with a uniform heat flux. The performance of every optimum design was assessed both at its optimization conditions, and with the other heat flux distributions applied.

2.3.2. Heat flux and coolant flow rate magnitude

The optimization was performed with standard boundary conditions of 500 W m⁻² heat flux and 0.001 kg s⁻¹ coolant flow rate. Additional optimizations were performed at heat flux magnitudes of 200 and 1000 W m⁻²; and coolant flow rates of 0.0004 and 0.002 kg s⁻¹, while keeping the other boundary condition constant. Table 2 shows all boundary conditions used in this study.

3. Numerical results

We considered variation of three boundary conditions—the non-uniform heat flux distribution type, the coolant mass flow rate, and the magnitude of heat flux. In actual vehicle design, the heat flux distribution type will be dictated by the orientation of the battery cell, which means the heat flux type will be fixed during vehicle operation. The coolant flow rate and heat flux magnitude, on the other hand, may change during operation depending on driving conditions, such as acceleration, speed, ambient temperature, and the use of climate control.

Section 3.1 considers various non-linear heat flux distribution types. As discussed in the Introduction, we will conduct a two-stage

Table 2
Summary of analysis boundary conditions.

Boundary condition name	Heat flux		Coolant flow rate (kg s ⁻¹)	Corresponding figures
	Gradient	Average magnitude (W m ⁻²)		
Reference BC	Uniform	500	0.001	4, 10b, 11b, 12b, 13b, 14b, 15b
BC 1(+y)	+y	500	0.001	6a, 7a, 8a
BC 1(-y)	-y	500	0.001	6b, 7b, 8b
BC 1(+x)	+x	500	0.001	6c, 7c, 8c
BC 1(-x)	-x	500	0.001	6d, 7d, 8d
BC 2	Uniform	500	0.0004	10a, 11a, 12a, 15a
BC 3	Uniform	500	0.002	10c, 11c, 12c, 15c
BC 4	Uniform	200	0.001	13a, 14a
BC 5	Uniform	1000	0.001	13c, 14c

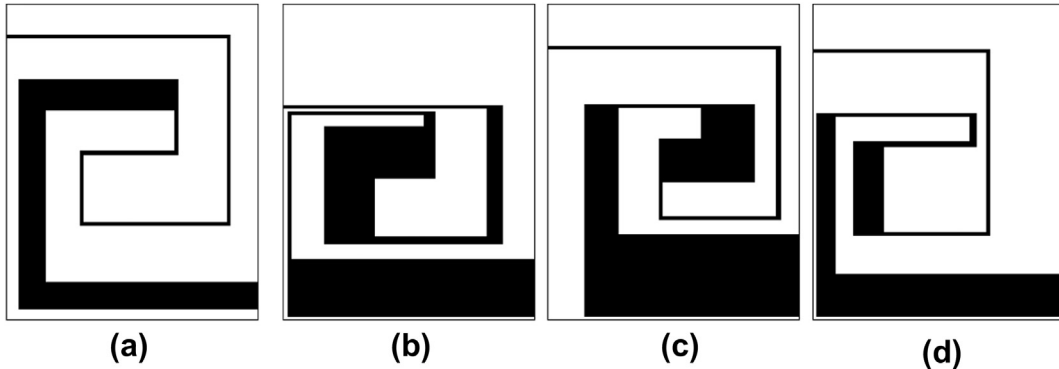


Fig. 6. Cooling plate geometry of four designs optimized for T_σ with non-uniform heat flux distributions of BC 1: average heat flux of 500 W m^{-2} , and coolant flow rate of 0.001 kg s^{-1} . (a) T_σ -optimized design with BC 1(+y). (b) T_σ -optimized design with BC 1(-y). (c) T_σ -optimized design with BC 1(+x). (d) T_σ -optimized design with BC 1(-x).

analysis. First, it will be shown how optimum solutions change according to various heat flux distribution types. Second, each optimum design will be exposed to a heat flux distribution that was not used to find that optimum design. Performance metrics at various off-design boundary conditions will then be discussed.

Section 3.2 considers various coolant flow rate values and heat flux magnitudes with a focus on the first aspect: finding optimum solutions at various different coolant flow rates and heat flux magnitudes, and comparing these optimum designs. Section 3.3 will discuss how optimum designs perform at

off-design boundary conditions in terms of the coolant flow rate and heat flux magnitude.

3.1. Optimum designs with different heat flux distributions and their performance at off-design boundary conditions

The optimum cooling plate designs with an objective function of T_σ subject to the four heat flux gradients of BC 1 are shown in Fig. 6. In all cases the position of the cooling channel is skewed towards the location of highest heat generation. For example in the plate

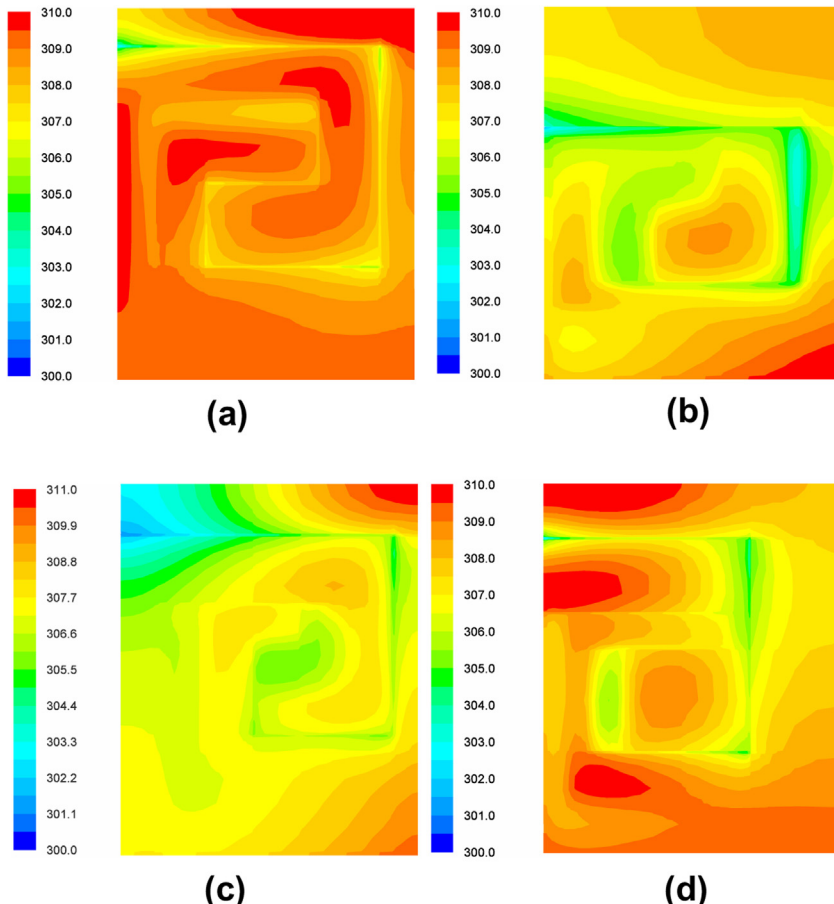


Fig. 7. Temperature distribution of four designs optimized for T_σ with non-uniform heat flux distributions of BC 1: average heat flux of 500 W m^{-2} , and coolant flow rate of 0.001 kg s^{-1} . (a) Temperature of T_σ -optimized design with BC 1(+y). (b) Temperature of T_σ -optimized design with BC 1(-y). (c) Temperature of T_σ -optimized design with BC 1(+x). (d) Temperature of T_σ -optimized design with BC 1(-x).

Table 3

Performance of cooling plates optimized with respect to T_σ with non-uniform heat flux boundary conditions. Values show performance at the optimum conditions.

Flux distribution	P_{fluid} (Pa)	T_{avg} (K)	T_σ (K)
+y	25,464	308.86	1.17
-y	19,098	307.15	1.64
+x	20,047	307.17	1.46
-x	23,457	308.13	1.48
Uniform	25,124	308.31	1.22

optimized using the positive y gradient heat flux (i.e. BC 1(+y)), the position of the top section of channel is closer to the top edge (positive y direction) than in any other designs. Conversely, in the design optimized using the negative y gradient (BC 1(−y)), the channel is located mostly in the bottom half of the plate. The same features can be seen in the optimizations using the x direction heat fluxes.

The temperature distributions of the four optimum designs of Fig. 6 are shown in Fig. 7. As a result of the optimization process, the position of the cooling channel has changed to most equalize the temperature over the plate. However, some of the designs have a more uniform temperature than others, and this is confirmed by Table 3, which states the performance of each of the five optimization designs subject to the five different boundary conditions. Note that the same objective function (i.e. standard deviation of temperature, T_σ) was used for all five designs. Both the temperature distributions and the performance data indicate that the lowest temperature variation is achieved with the heat flux gradient in the positive y direction (BC 1(+y)). This even gives a marginally better result than the optimization with a uniform heat flux (Reference BC). The least favourable orientation with respect to temperature uniformity is the negative y direction (BC 1(−y)).

The optimum cooling plate designs with an objective function of T_{avg} subject to BC1 are shown in Fig. 8. In these cooling plates, there is an absence of a consistent characteristic as seen in the designs optimized with respect to T_σ ; the channels are either spread out over the plate, or squashed in the middle with no correspondence to the heat flux distribution. The performance of each optimum plate is shown in Table 4; this shows that the ranking of the heat flux orientations is reversed in the case of T_{avg} optimizations. The design optimized with a negative y gradient leads to the lowest average temperature, and the design optimized with a positive y gradient performs worst.

To assess the robustness of the optimum designs, each optimum design was analyzed with boundary conditions that are different from the boundary condition used for optimization. For example, the design optimized with a −y gradient (BC 1(−y)) was analyzed

Table 4

Performance of cooling plates optimized with respect to T_{avg} with non-uniform heat flux boundary conditions. Values show performance at the optimum conditions.

Flux distribution	P_{fluid} (Pa)	T_{avg} (K)	T_σ (K)
+y	1773	306.55	2.47
-y	1526	303.82	2.87
+x	7983	304.77	2.11
-x	1795	304.89	3.22
Uniform	1232	305.25	2.32

with a +y heat flux gradient (BC 1(+y)) and uniform heat flux (Reference BC). The outcome of these assessments is shown in Fig. 9. The most obvious trend is seen in Fig. 9a and b, which relate to the optimizations with respect to T_σ : at every analysis condition, the design that performs best was the one optimized with the same heat flux distribution. As an example, the red dotted line in Fig. 9a represents the performance of the cooling plate design that is optimized for T_σ subject to BC 1(−y). If this design is subject to the same boundary condition, BC 1(−y), the temperature standard deviation is 1.6 K. However, if the same design is subject to BC 1(+y) the temperature standard deviation is close to 7 K. In some cases, the penalty for not optimizing with the appropriate boundary condition was a factor of two or more.

Fig. 9c shows the performance of the designs optimized with respect to T_{avg} using heat flux distributions in the +y/−y directions. Although there is some difference in performance between the three designs, the more significant trend is that all designs perform best (i.e. lowest average temperature) when a negative y heat flux is applied; with a positive y heat flux all designs have an average temperature at least 2 K higher. The designs optimized with respect to T_{avg} using heat flux distributions in the +x/−x directions (Fig. 9d) display similar behaviour as the T_σ designs: at every analysis condition, the design that performs best was the design optimized using the same conditions.

Fig. 9a and b suggests that for an optimum cooling plate design that is optimized for a particular non-uniform heat generation profile, its thermal performance in terms of temperature uniformity will become significantly sub-optimum if a different non-uniform heat generation profile is used. In order to achieve maximum possible temperature uniformity, it is important to use a design that is optimized for the particular heat flux distribution to experience. In other words, the temperature uniformity performance of a fixed optimum cooling plate design will not be robust against varying heat flux profiles in the x- or y-directions.

Similarly, Fig. 9d indicates that the average temperature performance of an optimum design is not robust either, with respect to varying heat flux profiles in the x-direction. With various

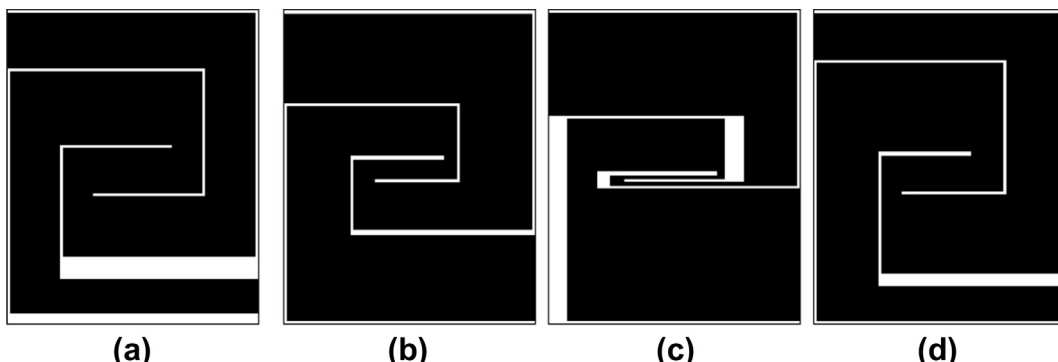


Fig. 8. Cooling plate geometry of four designs optimized for T_{avg} with non-uniform heat flux distributions of BC 1: average heat flux of 500 W m^{-2} , and coolant flow rate of 0.001 kg s^{-1} . (a) T_{avg} -optimized design with BC 1(+y). (b) T_{avg} -optimized design with BC 1(−y). (c) T_{avg} -optimized design with BC 1(+x). (d) T_{avg} -optimized design with BC 1(−x).

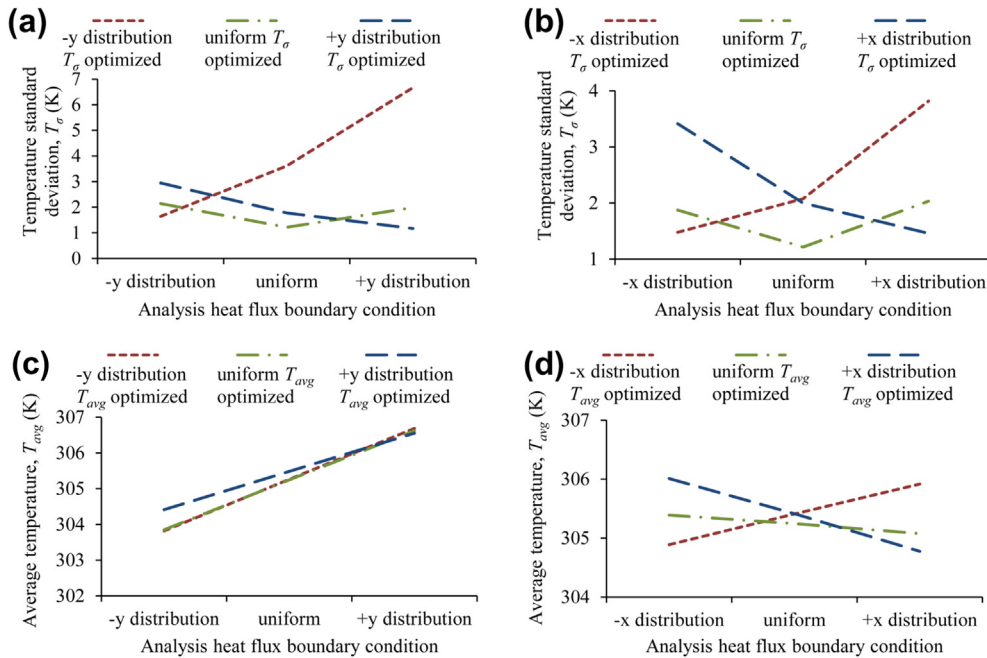


Fig. 9. Performance of cooling plates optimized with non-uniform heat flux boundary conditions of BC 1. Each chart shows the performance of plates at three conditions: their optimization condition, and two others. (a) T_σ performance of plates optimized with different heat flux gradients in the y direction. (b) T_σ performance of plates optimized with different heat flux gradients in the x direction. (c) T_{avg} performance of plates optimized with different heat flux gradients in the y direction. (d) T_{avg} performance of plates optimized with different heat flux gradients in the x direction.

y-directional heat generation profiles, one optimum solution will perform well in terms of minimum average temperature at off-design conditions.

3.2. Optimum designs with varying coolant flow rate and heat flux magnitude

To compare the cooling plate geometries optimized at different flow rates, Figs. 10–12 show the T_σ , T_{avg} , and P_{fluid} optimized designs respectively. A uniform heat flux of 500 W m^{-2} is applied in all cases. The T_σ designs in Fig. 10 display a clear trend in the position of the top channel section: as the coolant flow rate increases, the top channel section moves closer to the top edge of the plate. The mechanism behind this behaviour will be discussed in Fig. 15. The other channel sections also display some variation, but this may just be random variation—as seen in previous studies [11]. The

T_{avg} optimized designs in Fig. 11 show some variation in geometry but no noticeable trends, and the P_{fluid} optimized designs in Fig. 12 are almost identical.

The T_σ and T_{avg} optimized designs at different values of uniform heat flux are shown in Figs. 13 and 14 (P_{fluid} was not used as an objective function as it was not considered to be significantly affected by the heat flux boundary condition.). In both cases there seem to be no obvious trend in the designs—some variability is to be expected given the outcome of the study into the initial design dependence. Table 5 shows the numerical values of the thermal performance of optimum designs for T_σ and T_{avg} subject to four different boundary conditions used in Figs. 10–14.

The clearest trend observed from these additional optimizations was in the T_σ designs at different flow rates, as shown in Fig. 10. To better understand the mechanism driving the optimum design, the temperature distribution of T_σ -optimized designs at three different

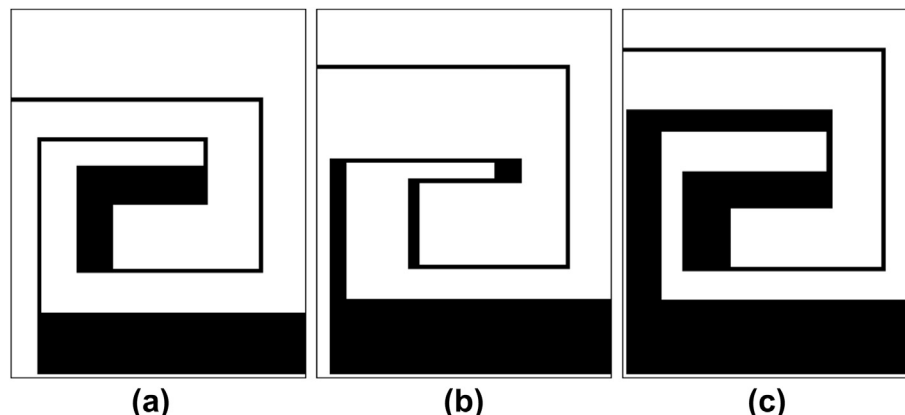


Fig. 10. Cooling plate geometry of T_σ -optimized designs at three different coolant flow rates. For all three cases, a uniform heat flux of 500 W m^{-2} is applied. (a) T_σ -optimized design with BC 2 (0.0004 kg s^{-1}). (b) T_σ -optimized design with Reference BC (0.001 kg s^{-1}). (c) T_σ -optimized design with BC 3 (0.002 kg s^{-1}).

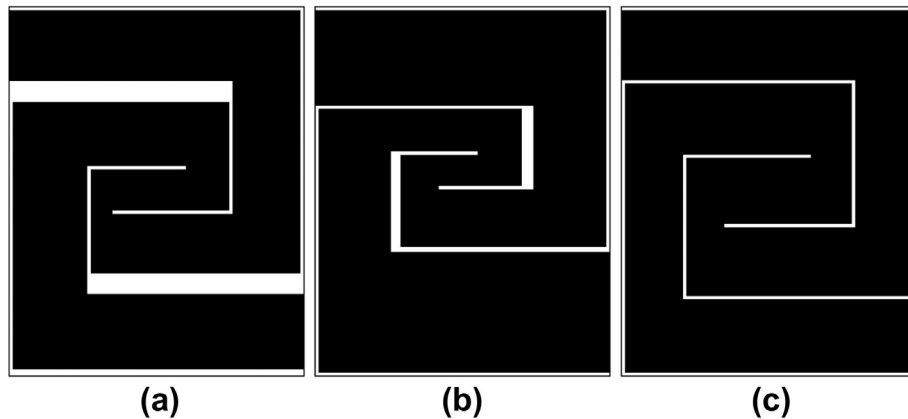


Fig. 11. Cooling plate geometry of T_{avg} -optimized designs at three different coolant flow rates. For all three cases, a uniform heat flux of 500 W m^{-2} is applied. (a) T_{avg} -optimized design with BC 2 (0.0004 kg s^{-1}). (b) T_{avg} -optimized design with Reference BC (0.001 kg s^{-1}). (c) T_{avg} -optimized design with BC 3 (0.002 kg s^{-1}).

coolant flow rates are shown in Fig. 15. As the coolant flow rate increases, it retains more of its cooling effect through the length of the channel: at the lowest flow rate (Fig. 15a), only the first channel section provides effective cooling, and so this takes a position closer to the centre of the plate. At the highest flow rate (Fig. 15c), effective cooling is provided for at least half the channel length, and so these sections are spread more evenly over the plate—meaning that the first channel section is pushed towards the edge of the plate.

If this trend can be extrapolated, then it indicates that at a sufficiently high flow rate (in which the outlet temperature is not significantly below the inlet temperature), the optimum design with respect to T_{σ} would be one in which the channels are of a relatively uniform width and evenly distributed over the plate. In this case, the optimum T_{σ} design may start to more closely resemble the optimum designs of T_{avg} and P_{fluid} .

3.3. Thermal performance at off-design coolant flow rate and heat flux magnitude boundary conditions

During operation in an EV, a cooling plate will not operate at its design condition all of the time, therefore it is important to assess it at off-design boundary conditions. The other reason for this assessment was to determine if the cooling plate optimum design is dependent on the boundary conditions.

The charts in Fig. 16 show the performance (in terms of T_{σ} and T_{avg}) of the reference plate (Fig. 3) over a range of inlet flow rate and heat flux magnitude. Increasing the coolant flow rate reduces both

the output functions of T_{σ} and T_{avg} , whereas increasing the heat flux increases both these parameters. The efficacy of the optimized designs is illustrated by plotting their performance normalized against the performance of the reference design; these charts are shown in Fig. 17.

For example, Fig. 17a shows that at low flow rates, the T_{avg} design optimized at 0.002 kg s^{-1} has the highest T_{avg} (about 95% of the reference design); the design optimized at 0.001 kg s^{-1} has the lowest T_{avg} (about 86% of the reference design). As the flow rate increases, all three optimum designs improve relative to the reference design, but the 0.002 kg s^{-1} optimized design improves the most until at a flow rate of 0.003 kg s^{-1} , it has the lowest T_{avg} (about 75% of the reference design). In this case, although there is some indication that a different design should be selected depending on the operating conditions, all three designs perform similarly.

Theoretically, the 0.0004 kg s^{-1} optimized design must perform best at 0.0004 kg s^{-1} . As the figure shows, however, the 0.001 kg s^{-1} optimized design performs slightly better than the 0.0004 kg s^{-1} optimized design at 0.0004 kg s^{-1} . This is because the optimization algorithm found only local optimum solutions due to the highly complex design space. All optimizations in this study started from the same initial design: the Reference geometry shown in Fig. 3. Fig. 1a7 indicates that the optimization with the boundary condition of 0.001 kg s^{-1} found an effective local optimum solution which performs best at 0.001 kg s^{-1} and at other flow rates as well. However, the performance difference between the 0.001 kg s^{-1}

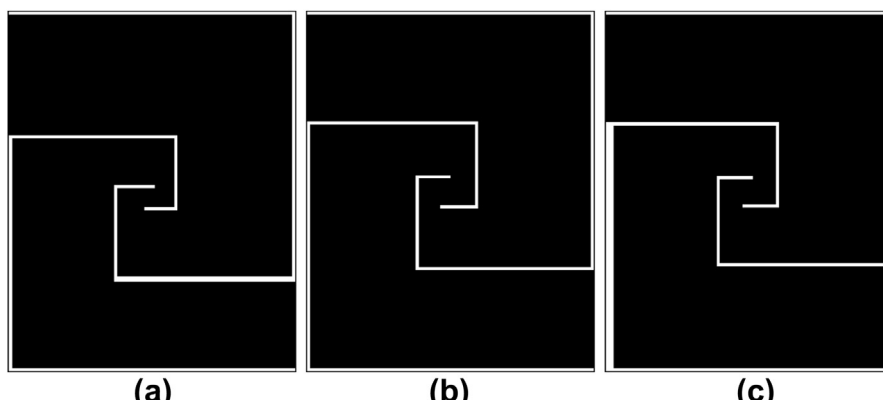


Fig. 12. Cooling plate geometry of P_{fluid} -optimized designs at three different coolant flow rates. For all three cases, a uniform heat flux of 500 W m^{-2} is applied. (a) P_{fluid} -optimized design with BC 2 (0.0004 kg s^{-1}). (b) P_{fluid} -optimized design with Reference BC (0.001 kg s^{-1}). (c) P_{fluid} -optimized design with BC 3 (0.002 kg s^{-1}).

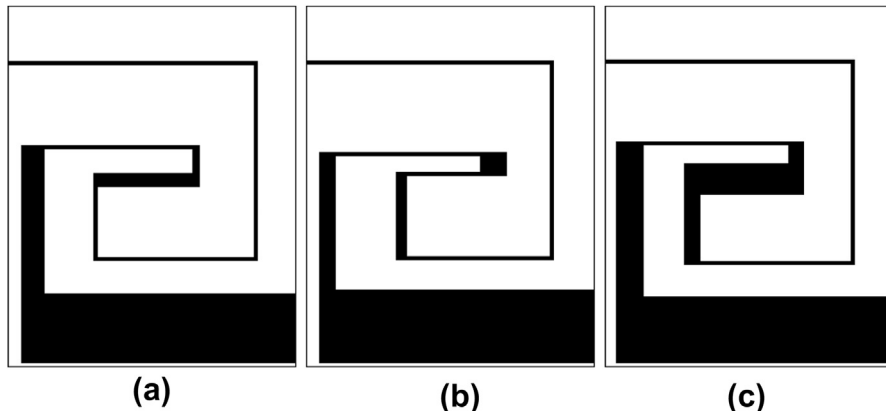


Fig. 13. Cooling plate geometry of T_{σ} -optimized designs at three different heat flux values. For all three cases, coolant flow rate is 0.001 kg s^{-1} . (a) T_{σ} -optimized design with BC 4 (uniform 200 W m^{-2}). (b) T_{σ} -optimized design with Reference BC (uniform 500 W m^{-2}). (c) T_{σ} -optimized design with BC 5 (uniform 1000 W m^{-2}).

optimized design and 0.0004 kg s^{-1} optimized design at 0.0004 kg s^{-1} is not significant (less than 5%).

The T_{σ} optimized designs shown in Fig. 17b present a distinctively different trend. Here it can be seen that the design optimized at 0.0004 kg s^{-1} performs best at low flow rates, the 0.001 kg s^{-1} design performs best at flow rates around 0.001 kg s^{-1} , and at higher flow rates, the 0.002 kg s^{-1} design is superior. Furthermore, away from their optimization conditions, in other words at off-design boundary conditions, their performance is significantly degraded, although the magnitude of this effect differs among the designs: the performance of the 0.0004 kg s^{-1} design is restricted to low flow rates, but the 0.002 kg s^{-1} design has acceptable (better than reference) performance over the entire tested range. Note the large variance in the y-axis in Fig. 17b, compared to the small range in Fig. 17a and very small ranges in Fig. 17c and d.

Variation in the heat flux boundary condition has almost no effect on the normalized performance of the optimum cooling plates. The T_{avg} optimized designs have a performance at about 87% of the reference design, and this is constant at all heat flux boundary conditions. The T_{σ} optimized designs show a small variation in the normalized value of T_{σ} .

4. Discussion and limitations

4.1. Discussion

The results of the study presented here indicate that there are two aspects of cooling plate design that need to be considered

when non-uniform heat generation is present. The first is regarding the desirable orientation of the cooling channels with respect to the distribution of heat generation: as shown in Fig. 7 and Table 3, the most uniform temperature was achieved when the inlet of the channel coincided with the region of greatest heat generation (in this case, the positive y gradient). In this situation, the greatest cooling force is applied to the region of the plate with the highest temperature, and the lower temperature regions receive the least cooling. However, for the lowest average temperature, the opposite condition was required as can be seen in Table 4: the channel inlet should be located on the side of lowest heat generation. No single inlet–outlet orientation performs best for both average temperature and temperature uniformity. With the trade-off, a design decision will have to be made considering relative importance of these two performance metrics.

The second aspect is regarding performance robustness with respect to variable heat flux distribution. In the case of the T_{σ} optimization, there is a significant advantage to be gained in optimizing the plate with the appropriate boundary condition. For example, Fig. 9a and b shows the potential for a very high penalty in T_{σ} if the heat flux gradient applied is opposite to that which the plate was optimized for. However, using a uniform heat flux for the optimization gives a consistently low (although non-optimum) value of T_{σ} no matter which operating boundary condition is applied, making it an attractive choice if the distribution of heat flux is not constant or unknown.

For T_{avg} optimized designs, there is less of an advantage to be gained by optimizing the design with the appropriate boundary

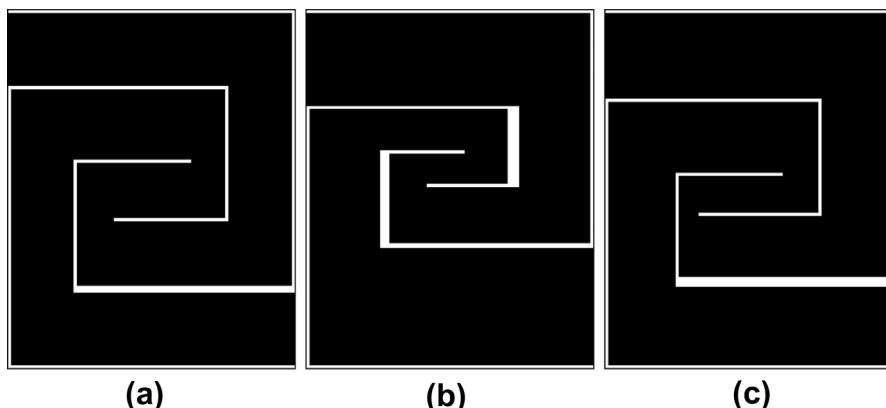


Fig. 14. Cooling plate geometry of T_{avg} -optimized designs at three different heat flux values. For all three cases, coolant flow rate is 0.001 kg s^{-1} . (a) T_{avg} -optimized design with BC 4 (uniform 200 W m^{-2}). (b) T_{avg} -optimized design with Reference BC (uniform 500 W m^{-2}). (c) T_{avg} -optimized design with BC 5 (uniform 1000 W m^{-2}).

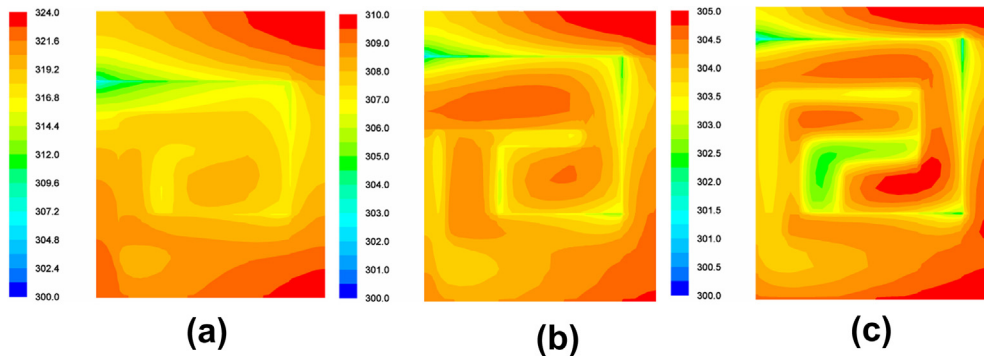


Fig. 15. Temperature distribution of T_σ -optimized designs at three different coolant flow rates. For all three cases, a uniform heat flux of 500 W m^{-2} is applied. (a) Temperature of T_σ -optimized design with BC 2 (0.0004 kg s^{-1}). (b) Temperature of T_σ -optimized design with Reference BC (0.001 kg s^{-1}). (c) Temperature of T_σ -optimized design with BC 3 (0.002 kg s^{-1}).

condition. Fig. 9c shows that there is a negligible benefit (approximately 1%) to be gained in optimizing with the correct heat flux gradient in the y direction. The heat flux gradients in the x direction exhibit a greater benefit from optimization with the appropriate boundary condition: up to 10% compared with the uniform design, shown in Fig. 9.

As noted in the assessment of off-design conditions (and seen in Figs. 12 and 17a and c), the optimizations of P_{fluid} and T_{avg} are generally insensitive to the magnitude of the boundary conditions (coolant flow rate and heat flux); i.e. a design optimized with one set of boundary conditions is also an optimum design at a different set of conditions. In contrast, the optimization of T_σ is sensitive to the heat flux distribution type (discussed above) and the coolant flow rate used in the optimization process (see Fig. 17b). However, for the heat flux magnitude boundary condition, the optimization of T_σ is insensitive, and it appears that one design will be an optimum at any heat flux magnitude.

(Note that these trends cannot necessarily be extrapolated beyond the flow rates and heat fluxes used in this study; the onset of unsteady flow, turbulence, or changing fluid properties could alter the optimum designs.)

These principles and guidelines can be used by cooling systems designers to tailor their design processes to achieve the optimum performance in their desired objective functions without going through unnecessary design phases and time-consuming optimization routines.

4.2. Limitations and further work

4.2.1. Cooling plate design

This study and the principles derived from it were all based on the assessment of one category of cooling plate: a single channel serpentine design. Although it is likely that similar design rules will

apply to other cooling plates, extrapolation becomes less reliable for significantly different designs; e.g. designs with multiple or branching channels. Furthermore, cooling plates of this shape are only of use with a battery pack of thin laminate cells; similar cooling considerations would be applicable to other battery cell formats, but the cooling design would be significantly different.

4.2.2. Boundary condition range

The range of boundary conditions was selected after discussion with our industrial partner, General Motors Canada. They were chosen to be representative of standard operating conditions. However, there is a limited range of boundary condition values.

Beyond the range selected, we could consider two situations: (1) a small extension beyond the simulated conditions, in which thermal and fluid mechanisms operate in the same regime; and (2) a large departure from the simulated conditions, in which fluid behaviour might be substantially different.

In the first case, we expect our results to be valid, and any trends identified can be safely extrapolated to the modified boundary conditions. In the second case, we may find that using the present model results in unrealistic response, due to changes in fluid behaviour or other physical mechanisms. This would require a re-examination of fluid and thermal parameters to check e.g. the turbulence model, followed by a re-verification of the CFD results.

4.2.3. Boundary condition interactions

In this study, we did not explicitly consider the interaction among multiple parameters: as an example, what would be the optimum design for average temperature if you change the flow rate and heat flux magnitudes simultaneously. However, from the results already presented we can make several reasonable conclusions regarding interaction of different analysis parameters:

4.2.3.1. Pressure drop. Considering the problem with respect to the objective function, we can initially exclude the pressure drop function from further discussion: all optimizations resulted in the same optimum design, regardless of boundary condition. Therefore, it is a reasonable expectation that some combination of these boundary conditions would not give a different result.

4.2.3.2. Average temperature. For the average temperature objective function, we surmised that even at different flow rates and heat flux magnitudes, there was a single design that would perform optimally with a uniform heat flux boundary condition. Therefore, in this situation, there is presumably no additional interaction between boundary conditions. Only when the optimization was performed with non-uniform heat flux boundary

Table 5

Performance of cooling plates optimized at additional boundary conditions. Results are for the performance at the conditions shown.

Objective function	Heat flux (W m^{-2})	Flow rate (kg s^{-1})	P_{fluid} (Pa)	T_{avg} (K)	T_σ (K)
T_σ	500	0.0004	3130	319.33	2.95
	500	0.002	46,901	304.11	0.75
	200	0.001	27,345	303.28	0.49
	1000	0.001	20,535	315.94	2.47
	500	0.0004	481	313.82	6.31
	500	0.002	3438	302.73	1.33
	200	0.001	1618	302.15	1.04
	1000	0.001	1283	310.55	4.95

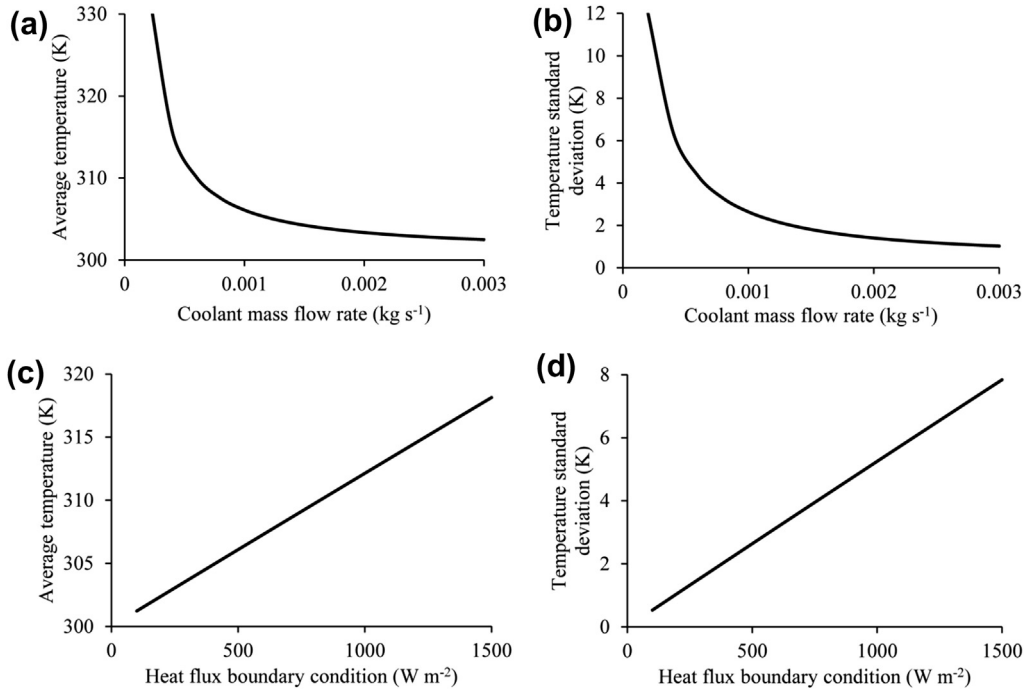


Fig. 16. Performance of the reference cooling plate at a range of flow rates and heat flux. (a) T_{avg} output at variable flow rates. (b) T_σ output at variable flow rates. (c) T_{avg} output at variable heat flux. (d) T_σ output at variable heat flux.

conditions was there evidence for sensitivity of the average temperature objective function. In summary, it appears that the average temperature optimum is sensitive to heat flux distribution, but not to magnitude or coolant flow rate. Therefore, we

could expect that variation in flow rate or heat flux magnitude would not affect the optimum solution for a given non-uniform heat flux boundary condition, but this would need to be further verified.

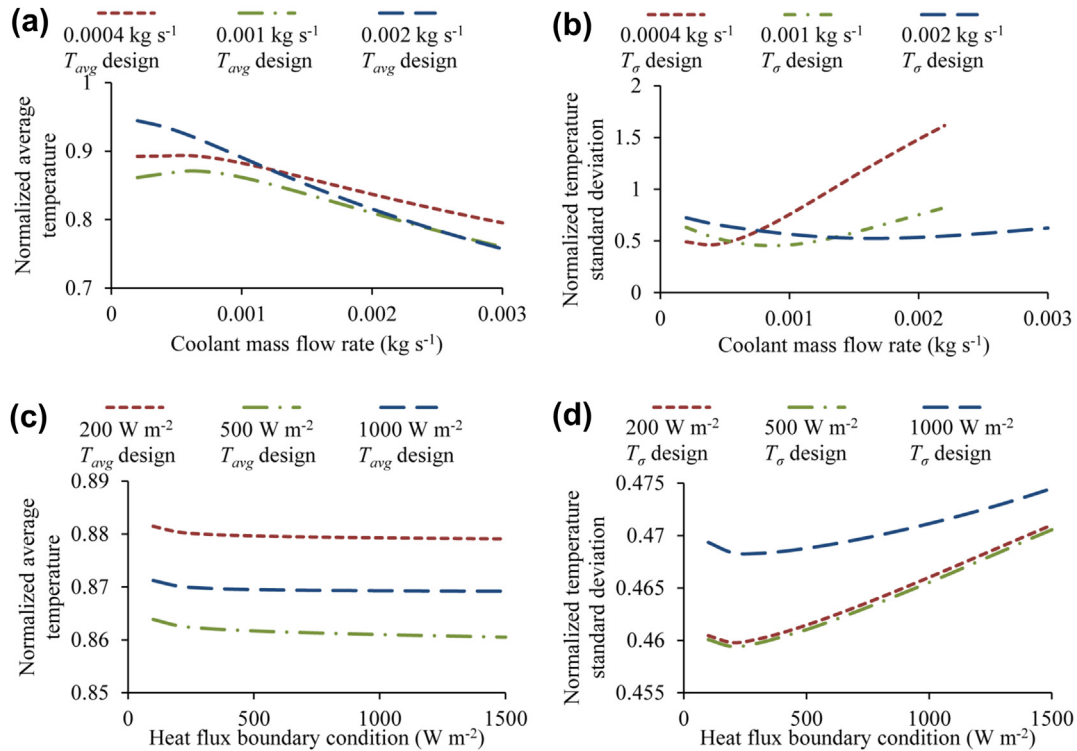


Fig. 17. Performance of optimized cooling plates at a range of flow rates and heat flux. The cooling plate performance is normalized against the reference cooling plate performance in Fig. 16. (a) Performance of T_{avg} optimized designs at variable flow rates. (b) Performance of T_σ optimized designs at variable flow rates. (c) Performance of T_{avg} optimized designs at variable heat flux. (d) Performance of T_σ optimized designs at variable heat flux.

4.2.3.3. Temperature uniformity. The third objective function is the temperature uniformity. This was shown to be sensitive to both the heat flux distribution, and the coolant flow rate; and so is the most interesting example to choose. By generalizing the influence of each boundary condition, we can make some predictions about their interaction. The effect of applying a non-uniform heat flux distribution is to skew the cooling channel towards the area(s) of highest heat generation. This result is intuitive, and we believe that it would be seen in a general case. The effect of increasing the coolant flow rate is to make the cooling channel more uniformly effective, therefore its distribution on the plate (assuming uniform heat generation) becomes more evenly spaced, and its width shows less variation.

If the effect of these two boundary conditions combines with negligible interaction, then introducing non-uniformity into the heat flux distribution will skew the cooling channel, while increasing the flow rate will make the channel more uniform. However, in the case of non-uniform heat generation, it does not seem logical that by increasing the flow rate, the cooling channel would ultimately become perfectly uniform; rather, that it will have a uniform geometry superimposed on the heat generation distribution. This hypothesis would need to be verified by further optimization trials.

4.2.4. Vehicle operating condition

Although the purpose of this study was to investigate the influence of different boundary conditions on the optimum design, its scope was limited to a number of discrete conditions assessed by steady state analysis. In operation, an electric vehicle battery is exposed to a wide range of operating conditions including transient thermal behaviour, for example while warming up on a cold day. Ideally, the design process should take account of the full range of transient conditions, but due to computing restrictions and complexity, this was infeasible. However, a more elaborate optimization process could be formulated that would perform multiple objective function evaluations at different conditions, and weight them according to the time spent in the operating regime.

4.2.5. Analysis model

The model used in this study included only a cooling plate, and the behaviour and measurement of the battery state was deduced from the temperature on the cooling plate surface. However, this can only approximate the true battery behaviour and temperature; in order to increase the accuracy of the analysis, the CFD model should include the battery, heat generation, and contact conductance. The thermal objective functions can then be measured over the volume of the battery, rather than on the face of the cooling plate. Furthermore, a more elaborate model would allow the investigation into the interdependence of temperature and heat generation that exists in battery cells.

5. Conclusions

This study has investigated the process of designing EV battery cooling plates by assessing the sensitivity of the optimum design to the cooling plate boundary conditions. We found that the design was most sensitive when an objective function or boundary condition was considered involving the temperature uniformity.

The optimization of uniform temperature was very sensitive, both to the distribution of heat generated by the battery, and to the coolant flow rate. Optimization of average temperature was significantly sensitive only to the heat flux distribution. Finally, optimization of the pressure drop objective was sensitive to none of the tested boundary conditions.

Although this study was undertaken using a single channel serpentine cooling plate with fixed topology, these guidelines (or similar) are expected to apply to other cooling plate designs. Their application to the cooling system design process will identify the critical optimization activities and prevent unnecessary duplication of other optimizations. For example, if two different battery packs are being designed, and the primary requirement for the battery cells is control of the average temperature, then the only case in which different cooling plate designs might be required is if the distribution of battery heat generation differs. Alternately, if the design of a battery pack requires highly uniform temperature in the battery cells, and its operation encompasses a range of coolant flow rates, then the design of a single cooling plate should involve optimization at multiple flow rates.

Limitations of the design space and the boundary condition scope have been identified, but this study will still provide vehicle engineers with a useful tool in formulating the battery pack design process. With appropriate optimization tools, this will allow them to determine the optimum design more accurately and with less design work.

Acknowledgements

This research is funded by AUTO21, a member of the Network of Centres of Excellence of Canada program. Technical advice and direction was gratefully received from Derrick Chow, Brian Tossan, Justin Gammage, Carlton Fuerst, and colleagues at GM Canada.

References

- [1] A.A. Pesaran, A. Vlahinos, S.D. Burch, Thermal Performance of EV and HEV Battery Modules and Packs, in: Proceedings of the 14th International Electric Vehicle Symposium, Orlando, Florida (December 15–17, 1997).
- [2] A.A. Pesaran, S.D. Burch, M. Keyser, An Approach for Designing Thermal Management Systems for Electric and Hybrid Vehicle Battery Packs, in: Proceedings of the 4th Vehicle Thermal Management Systems Conference and Exhibition (1999), pp. 24–27.
- [3] A. Pesaran, M. Keyser, Thermal characteristics of selected EV and HEV batteries, in: Applications and Advances, 2001, The Sixteenth Annual Battery Conference on, IEEE, 2001, pp. 219–225.
- [4] A. Pesaran, G. Kim, M. Keyser, Integration Issues of Cells into Battery Packs for Plug-In and Hybrid Electric Vehicles, in: 24th International Batterie, Hybrid and Fuel Cell Electric Vehicle Symposium (EVS24), Stavanger (2009).
- [5] U.S. Kim, C.B. Shin, C.S. Kim, J. Power Sources 189 (1) (2009) 841–846.
- [6] K. Smith, G.H. Kim, A.A. Pesaran, Modeling of Nonuniform Degradation in Large Format Li-ion Batteries, in: Presented at the Advanced Automotive Battery and EC Capacitor Conference (2009).
- [7] N. Shidore, T. Bohn, Evaluation of Cold Temperature Performance of the JCS-VL41M PHEV Battery Using Battery HIL, Tech. Rep. 2008-01-1333, SAE, 2008.
- [8] X. Hu, S. Li, H. Peng, F. Sun, J. Power Sources 217 (2012) 209–219.
- [9] U.S. Kim, J. Yi, C.B. Shin, T. Han, S. Park, J. Electrochem. Soc. 158 (5) (2011) A611–A618.
- [10] S. Jayaraman, G. Anderson, S. Kaushik, P. Klaus, Modeling of Battery Pack Thermal System for a Plug-in Hybrid Electric Vehicle, Tech. Rep. 2011-01-0666, SAE, 2011.
- [11] A. Jarrett, I.Y. Kim, J. Power Sources 196 (23) (2011) 10359–10368.
- [12] S.H. Yu, S. Sohn, J.H. Nam, C.J. Kim, J. Power Sources 194 (2) (2009) 697–703.
- [13] H.H. Bau, Int. J. Heat Mass Transf. 41 (18) (1998) 2717–2723.